(Received 3 February 2024, Accepted 16 April 2024, Scheduled May 10 2024)

Electromagnetically Induced Transparency and Fano Resonances in Waveguides and U-Shaped or Cross-Shaped Resonators

Tarik Touiss[1,*], Ilyass El Kadmiri[1,2], Younes Errouas[1], and Driss Bria[1]

[1]*Laboratory of Materials, Waves, Energy and Environment*
Team of Waves, Acoustics, Photonics and Materials, Mohamed I University, Oujda, Morocco
[2]*Laboratory of Computer Science and Interdisciplinary Physics, ENSF*
Sidi Mohamed Ben Abdellah University, Fez, Morocco

ABSTRACT: In this paper, we study one-dimensional (1D) integrated photonic systems composed of waveguides connected to resonators. We explain and discuss the appearance of two unique resonance phenomena: Fano transparency and electromagnetically induced transparency (EIT). These resonances play a crucial role in optimizing signal filtering in photonic devices. Our study focuses on two geometrical configurations: a cross-shaped arrangement with collocated lateral resonators at the same site and a U-shaped configuration with resonators positioned at different sites. We use Transfer Matrix Method (TMM) to analyze these configurations, improving existing theoretical models for photonic waveguide systems. Using this method, we can manipulate the geometrical parameters of resonators to fine-tune the transmission properties associated with the Fano and EIT resonances. Our results indicate that symmetrical resonators eliminate Fano resonance in cross-shaped structures, while the introduction of asymmetrical resonators induces their emergence. For U-shaped structures, we demonstrate the presence of Fano and EIT resonances, and show that their manifestation depends on the geometric parameters of the resonators. Our research has two major implications: Firstly, it advances the theoretical knowledge of resonance phenomena in photonic waveguides. Secondly, it provides a methodology for the design of photonic structures with adapted transmission characteristics, opening the way to applications in advanced signal processing technologies.

1. INTRODUCTION

Rapid advances in photonics have brought to light numerous electromagnetic resonant phenomena, notably associated with the physics of electromagnetically induced interferences (EIT) and Fano resonances. These phenomena have important practical applications, particularly in the fields of electromagnetic switching and detection. An in-depth understanding of these resonant phenomena and their interconnections are crucial to the efficient design of electromagnetic devices.

Historically, EIT and Fano resonances [1–3] were first discovered in atomic systems, resulting from destructive interferences in excitation pathways to higher atomic levels. Their study has spread to other fields, with promising applications in the control of slow light. These phenomena are not limited to atomic systems and have been extensively studied in classical systems, including photonic waveguides [4–6]. An example of EIT resonance occurs in opaque atomic media. The coupling of photonic waveguides with one or more resonators has been studied and applied to obtain Fano and EIT-type resonances [6–13]. In transmission spectra, the Fano profile appears as a maximum transmission peak close to a transmission zero [14–16]. When the Fano resonance falls between two antiresonances (two transmission zeros), it becomes an EIT resonance. To generate such resonances in conventional systems, two or more resonators are usually connected to a waveguide, either directly or indirectly. Simple structures, such as cross or U-shaped structures, have demonstrated these resonances theoretically and experimentally. In addition, both the crossed and U-shaped structures have been proposed to study a Y-shaped photonic demultiplexer [17] based on EIT and Fano resonances. Mouadili et al. [6] have theoretically demonstrated that a simple structure composed of two lateral detuned photonic resonators grafted onto a tube can exhibit both Fano and EIT resonances by modifying the geometrical parameters of the resonators. Recent researches have revealed that the electromagnetic transmission spectrum of 1D comb-like waveguides structures presents large band gaps [18–20]. These structures are made up of periodic cells, each with lateral resonators. One of the main advantages of these structures is their ability to create large band gaps and passbands. Errouas et al. [21] have demonstrated the possibility of realizing an electromagnetic filter exploiting three defect modes in large band gaps by creating asymmetrical resonator defects in a star waveguide structure. Similarly, Ben-Ali et al. [22] have demonstrated the appearance of four defect modes in the band gap by creating resonator defects at two different sites.

The main objective of this work is to study and clarify the phenomena of electromagnetically induced transparency (EIT) and Fano resonances in different one-dimensional (1D) struc-

* Corresponding author: Tarik Touiss (tariktouiss22@gmail.com).

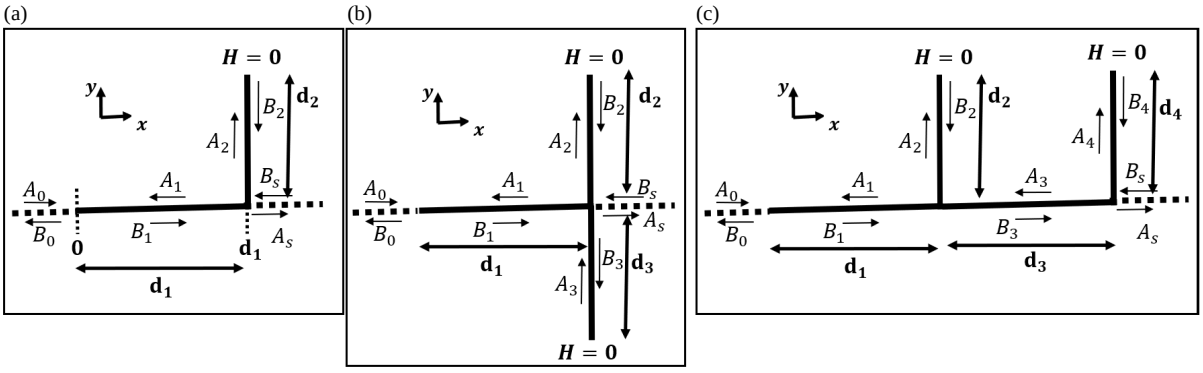

FIGURE 1. Schematic illustration of different waveguide and resonator structures: (a) Single-resonator waveguide with a resonator of length d_2 attached to a waveguide of length d_1. (b) Cross-shaped resonators structure integrated with a waveguide of length d_1, comprising two perpendicular resonators of lengths d_2 and d_3. (c) Dual waveguide system with U-shaped resonators, each waveguide of length d_1 and d_3 respectively, connected to resonators of lengths d_2 and d_4. All elements are made of identical materials.

tures, in particular waveguides integrated with U-shaped and cross-shaped resonators. This research aims to bridge the theoretical and practical aspects of photonics by demonstrating how these resonances can be exploited in 1D photonic systems to enhance the guiding and filtering capabilities of electromagnetic waves, thus contributing to the advancement of photonic devices. Using the transfer matrix method for a detailed analysis of wave propagation through these unique 1D structures, the study aims to provide a comprehensive understanding of waveguide-resonator interactions. In addition, this work aims to demonstrate the potential of these structures in improving the performance of photonic systems. Through a combination of theoretical analysis and experimental validation, the study aims to make a significant contribution to the field of photonics, opening up new ways for the design and development of advanced electromagnetic devices with enhanced functionality.

The paper is structured as follows. Section 2 explains how the Transfer Matrix Method (TMM) is used to calculate transmission and reflection rates. Section 3 presents the results of the calculations and a discussion of their implications, and Section 4 summarizes the main conclusions drawn from the results.

2. MODEL AND FORMALISM

In this section, we present our theoretical approach based on the transfer matrix method [23, 24] for analyzing the transmission of electromagnetic waves through a waveguide grafted by a resonator. The waveguides studied are coaxial cables with a dielectric permittivity ε. The boundary conditions applied to the ends of the resonator are of the type $H = 0$.

2.1. Case of a Waveguide of Length d_1 Grafted with a Resonator of Length d_2

In this subsection, we calculate the transfer matrix of a photonic system consisting of a waveguide of length d_1 grafted with a resonator of length d_2 (Fig. 1(a)).

The expressions of the electric fields in four media are given by:

$$E(x,y) = \begin{cases} E_0(x) = A_0 e^{j\alpha_0 x} + B_0 e^{-j\alpha_0 x} \\ \text{for}: \ x \le 0 \\ E_1(x) = A_1 e^{j\alpha_1 x} + B_1 e^{-j\alpha_1 x} \\ \text{for}: \ 0 \le x \le d_1 \\ E_s(x) = A_s e^{j\alpha_s (x-d_1)} + B_s e^{-j\alpha_s (x-d_1)} \\ \text{for}: \ x \ge d_1 \\ E_2(y) = A_2 e^{j\alpha_2 y} + B_2 e^{-j\alpha_2 y} \\ \text{for}: \ 0 \le y \le d_2 \end{cases} \quad (1)$$

By applying the boundary condition at the end of the resonator, the expression of the electric field within the resonator is modified as follows:

$$E_2(y) = G\cos(\alpha_2 (y - d_2)) \quad (2)$$

The passing conditions at $x = 0$:

$$\begin{cases} E_0(x=0) = E_1(x=0) \\ \dfrac{dE_0(x)}{dx}_{x=0} = \dfrac{dE_1(x)}{dx}_{x=0} \end{cases} \quad (3)$$

It can be written as:

$$\begin{pmatrix} 1 & 1 \\ \alpha_0 & -\alpha_0 \end{pmatrix} \begin{pmatrix} A_0 \\ B_0 \end{pmatrix} = \begin{pmatrix} 1 & 1 \\ \alpha_1 & -\alpha_1 \end{pmatrix} \begin{pmatrix} A_1 \\ B_1 \end{pmatrix} \quad (4)$$

The passing conditions at $y = 0$ and $x = d_1$ are given by:

$$\begin{cases} E_1(x=d_1) = E_s(x=d_1) = E_2(y=0) \\ \dfrac{dE_1(x)}{dx}_{x=d_1} = \dfrac{dE_s(x)}{dx}_{x=d_1} + \dfrac{dE_2(y)}{dy}_{y=0} \end{cases} \quad (5)$$

After calculating the system described in Eq. (5), we obtain:

$$\begin{pmatrix} A_1 \\ B_1 \end{pmatrix} = \frac{-1}{2\alpha_1}$$

$$\begin{pmatrix} -\alpha_1 e^{-j\alpha_1 d_1} + j\alpha_2 e^{-j\alpha_1 d_1} \tan(\alpha_2 d_2) & -e^{-j\alpha_1 d_1} \\ -\alpha_1 e^{j\alpha_1 d_1} - j\alpha_2 e^{j\alpha_1 d_1} \tan(\alpha_2 d_2) & e^{j\alpha_1 d_1} \end{pmatrix} \begin{pmatrix} 1 & 1 \\ \alpha_s & -\alpha_s \end{pmatrix} \begin{pmatrix} A_s \\ B_s \end{pmatrix} \tag{6}$$

By replacing the matrix $\begin{pmatrix} A_1 \\ B_1 \end{pmatrix}$, we find the resulting matrix of the guide-resonator system situated between two semi-infinite guides, which is given as follows:

$$\begin{pmatrix} 1 & 1 \\ \alpha_0 & -\alpha_0 \end{pmatrix} \begin{pmatrix} A_0 \\ B_0 \end{pmatrix} = \begin{pmatrix} \cos(\alpha_1 d_1) - \frac{\alpha_2}{\alpha_1} \tan(\alpha_2 d_2) \sin(\alpha_1 d_1) & -j \frac{\sin(\alpha_1 d_1)}{\alpha_1} \\ -j\alpha_1 \sin(\alpha_1 d_1) - j\alpha_2 \tan(\alpha_2 d_2) \cos(\alpha_1 d_1) & \cos(\alpha_1 d_1) \end{pmatrix} \begin{pmatrix} 1 & 1 \\ \alpha_s & -\alpha_s \end{pmatrix} \begin{pmatrix} A_s \\ B_s \end{pmatrix} \tag{7}$$

Subsequently, the G matrix, which includes all the interaction between the guide and resonator, is simplified as follows: $G = \begin{pmatrix} G_{11} & G_{12} \\ G_{21} & G_{22} \end{pmatrix}$, where the elements of G are defined as:

- $G_{11} = \cos(\alpha_1 d_1) - \frac{\alpha_2}{\alpha_1} \tan(\alpha_2 d_2) \sin(\alpha_1 d_1)$
- $G_{12} = -j \frac{\sin(\alpha_1 d_1)}{\alpha_1}$
- $G_{21} = -j\alpha_1 \sin(\alpha_1 d_1) - j\alpha_2 \tan(\alpha_2 d_2) \cos(\alpha_1 d_1)$
- $G_{22} = \cos(\alpha_1 d_1)$

The transmission and reflection coefficients are given by the following expressions:

$$\begin{cases} t = \dfrac{A_s}{A_0}_{B_s=0} = \dfrac{2}{(G_{11} + \alpha_s G_{12}) + \dfrac{1}{\alpha_0}(G_{21} + \alpha_s G_{22})} \\ r = \dfrac{B_0}{A_0}_{B_S=0} = \dfrac{(G_{11} + \alpha_s G_{12}) - \dfrac{1}{\alpha_0}(G_{21} + \alpha_s G_{22})}{(G_{11} + \alpha_s G_{12}) + \dfrac{1}{\alpha_0}(G_{21} + \alpha_s G_{22})} \end{cases} \tag{8}$$

The transmission and reflection rates are given by:

$$\begin{cases} T = |t|^2 = \left| \dfrac{2}{(G_{11} + \alpha_s G_{12}) + \dfrac{1}{\alpha_0}(G_{21} + \alpha_s G_{22})} \right|^2 \\ R = |r|^2 = \left| \dfrac{(G_{11} + \alpha_s G_{12}) - \dfrac{1}{\alpha_0}(G_{21} + \alpha_s G_{22})}{(G_{11} + \alpha_s G_{12}) + \dfrac{1}{\alpha_0}(G_{21} + \alpha_s G_{22})} \right|^2 \end{cases} \tag{9}$$

2.2. Maintaining the Integrity of the Waveguide of Length d_1 Grafted with Two Cross-Shaped Resonators of Lengths d_2 and d_3

In this subsection, we introduce a second resonator positioned at the same location as the first resonator. This creates a cross-shaped structure as illustrated in Fig. 1(b).

The electric fields expressions in all media are given by:

$$E(x,y) = \begin{cases} E_0(x) = A_0 e^{j\alpha_0 x} + B_0 e^{-j\alpha_0 x} \\ \text{for}: \ x \le 0 \\ E_1(x) = A_1 e^{j\alpha_1 x} + B_1 e^{-j\alpha_1 x} \\ \text{for}: \ 0 \le x \le d_1 \\ E_s(x) = A_s e^{j\alpha_s (x-d_1)} + B_s e^{-j\alpha_s (x-d_1)} \\ \text{for}: \ x \ge d_1 \\ E_2(y) = A_2 e^{j\alpha_2 y} + B_2 e^{-j\alpha_2 y} \\ \text{for}: \ 0 \le y \le d_2 \\ E_3(y) = A_3 e^{j\alpha_3 y} + B_3 e^{-j\alpha_3 y} \\ \text{for}: \ 0 \le y \le d_3 \end{cases} \tag{10}$$

We have already described the steps necessary to calculate the transfer matrix. In this case, we will go directly to the following transfer matrix:

$$K = \begin{pmatrix} K_{11} & K_{12} \\ K_{21} & K_{22} \end{pmatrix} \tag{11}$$

The expressions of the elements of the matrix K are:

$$\begin{cases} K_{11} = \cos(\alpha_1 d_1) - \dfrac{\alpha_2}{\alpha_1} \tan(\alpha_2 d_2) \sin(\alpha_1 d_1) \\ \qquad - \dfrac{\alpha_3}{\alpha_1} \tan(\alpha_3 d_3) \sin(\alpha_1 d_1) \\ K_{12} = -j \dfrac{\sin(\alpha_1 d_1)}{\alpha_1} \\ K_{21} = -j\alpha_1 \sin(\alpha_1 d_1) - j \dfrac{\alpha_2}{\alpha_1} \tan(\alpha_2 d_2) \cos(\alpha_1 d_1) \\ \qquad - \dfrac{\alpha_3}{\alpha_1} \tan(\alpha_3 d_3) \cos(\alpha_1 d_1) \\ K_{22} = \cos(\alpha_1 d_1) \end{cases} \tag{12}$$

The transmission and reflection rates are given by:

$$\begin{cases} T = \left| \dfrac{2}{(K_{11} + \alpha_s K_{12}) + \dfrac{1}{\alpha_0}(K_{21} + \alpha_s K_{22})} \right|^2 \\ R = \left| \dfrac{(K_{11} + \alpha_s K_{12}) - \dfrac{1}{\alpha_0}(K_{21} + \alpha_s K_{22})}{(K_{11} + \alpha_s K_{12}) + \dfrac{1}{\alpha_0}(K_{21} + \alpha_s K_{22})} \right|^2 \end{cases} \tag{13}$$

2.3. Two Waveguides Grafted with Two U-Shaped Resonators

In this subsection, we focus on a simple application of the transfer matrix to a U-shaped structure as illustrated in Fig. 1(c). We calculate the transfer matrix of a system composed of two

waveguides of lengths d_1 and d_3, each grafted with a resonator of lengths d_2 and d_4, respectively.

The electric field expressions are given by:

$$E(x,y) = \begin{cases} E_0(x) = A_0 e^{j\alpha_0 x} + B_0 e^{-j\alpha_0 x} \\ \text{for}: \ x \le 0 \\ E_1(x) = A_1 e^{j\alpha_1 x} + B_1 e^{-j\alpha_1 x} \\ \text{for}: \ 0 \le x \le d_1 \\ E_2(y) = A_2 e^{j\alpha_2 y} + B_2 e^{-j\alpha_2 y} \\ \text{for}: \ 0 \le y \le d_2 \\ E_3(x) = A_3 e^{j\alpha_3 x} + B_3 e^{-j\alpha_3 x} \\ \text{for}: \ d_2 \le x \le d_3 \\ E_S(x) = A_S e^{j\alpha_S x} + B_S e^{-j\alpha_S x} \\ \text{for}: \ x \ge d_3 \\ E_4(y) = A_4 e^{j\alpha_4 y} + B_4 e^{-j\alpha_4 y} \\ \text{for}: \ 0 \le y \le d_4 \end{cases} \tag{14}$$

In this situation, we will multiply two matrices corresponding to guides and resonators. These matrices are defined as follows in the case presented:

$$\begin{pmatrix} 1 & 1 \\ \alpha_0 & -\alpha_0 \end{pmatrix} \begin{pmatrix} A_0 \\ B_0 \end{pmatrix} =$$

$$\begin{pmatrix} \cos(\alpha_1 d_1) - \frac{\alpha_3}{\alpha_1}\tan(\alpha_3 d_3)\sin(\alpha_1 d_1) & -j\frac{\sin(\alpha_1 d_1)}{\alpha_1} \\ -j\alpha_1 \sin(\alpha_1 d_1) - j\frac{\alpha_3}{\alpha_1}\tan(\alpha_3 d_3)\cos(\alpha_1 d_1) & \cos(\alpha_1 d_1) \end{pmatrix}$$

$$\begin{pmatrix} 1 & 1 \\ \alpha_3 & -\alpha_3 \end{pmatrix} \begin{pmatrix} A_3 \\ B_3 \end{pmatrix} \tag{15}$$

$$\begin{pmatrix} 1 & 1 \\ \alpha_3 & -\alpha_3 \end{pmatrix} \begin{pmatrix} A_3 \\ B_3 \end{pmatrix} =$$

$$\begin{pmatrix} \cos(\alpha_3 d_3) - \frac{\alpha_4}{\alpha_3}\tan(\alpha_4 d_4)\sin(\alpha_3 d_3) & -j\frac{\sin(\alpha_3 d_3)}{\alpha_3} \\ -j\alpha_3 \sin(\alpha_3 d_3) - j\frac{\alpha_4}{\alpha_3}\tan(\alpha_4 d_4)\cos(\alpha_3 d_3) & \cos(\alpha_3 d_3) \end{pmatrix}$$

$$\begin{pmatrix} 1 & 1 \\ \alpha_s & -\alpha_s \end{pmatrix} \begin{pmatrix} A_s \\ B_s \end{pmatrix} \tag{16}$$

The matrix product mentioned can be represented by an alternative notation to simplify later calculations. We define $P = \begin{pmatrix} P_{11} & P_{12} \\ P_{21} & P_{22} \end{pmatrix}$. By applying this notation, we obtain:

$$\begin{pmatrix} 1 & 1 \\ \alpha_0 & -\alpha_O \end{pmatrix} \begin{pmatrix} A_0 \\ B_0 \end{pmatrix}$$

$$= \begin{pmatrix} P_{11} & P_{12} \\ P_{21} & P_{22} \end{pmatrix} \begin{pmatrix} 1 & 1 \\ \alpha_s & -\alpha_s \end{pmatrix} \begin{pmatrix} A_s \\ B_s \end{pmatrix} \tag{17}$$

The transmission and reflection rates are given by:

$$\begin{cases} T = \left| \dfrac{2}{(P_{11} + \alpha_s P_{12}) + \dfrac{1}{\alpha_0}(P_{21} + \alpha_s P_{22})} \right|^2 \\ R = \left| \dfrac{(P_{11} + \alpha_s P_{12}) - \dfrac{1}{\alpha_0}(P_{21} + \alpha_s P_{22})}{(P_{11} + \alpha_s P_{12}) + \dfrac{1}{\alpha_0}(P_{21} + \alpha_s P_{22})} \right|^2 \end{cases} \tag{18}$$

3. RESULTS AND DISCUSSIONS

In this section, we present a numerical analysis of the propagation of electromagnetic waves through a different system, focusing on the behavior of these waves in different mediums. We take the dielectric permittivity of the segments and resonators respectively as $\varepsilon_i = 2.3$ (polyethylene), and the magnetic permeability of the materials is $\mu_i = 1$ (non-magnetic medium), where 'i' indicates the medium ($i = [1-4]$). The reduced frequency is given by $\Omega = \frac{\omega D\sqrt{\varepsilon_i \mu_i}}{c}$ which is a dimensionless quantity, with D being a unit of length, c the velocity of electromagnetic waves in vacuum, and ω the pulsation.

3.1. Transmission and Reflection Spectra in the Case of a Waveguide Grafted with a Resonator

In this subsection, we will explore the impact of inserting a resonator. We consider a system composed of a waveguide grafted with a resonator (Fig. 1(a)). The lengths of the waveguide and resonator are noted as d_1 and d_2, respectively.

Figure 2 illustrates the variation of reflection (blue line) and transmission (red line) rates as a function of the reduced frequency Ω for two values of resonator lengths: $d_2 = 0.5D$ (Fig. 2(a)) and $d_2 = 1D$ (Fig. 2(b)), where $d_1 = 1D$. These figures show the maximum and minimum values for reflection and transmission rates. Fig. 2(a) shows that transmission peaks reach unity at reduced frequencies $\Omega = 6.29$ and fall to zero at $\Omega = 3.17$ and $\Omega = 9.4$. Conversely, the reflection rate shows the opposite trend. Similarly, the sum of reflection and transmission rates is equal to 1. According to Fig. 2(b), transmission reaches its maximum around the reduced frequencies $\Omega = 3.14$, $\Omega = 6.29$, and $\Omega = 9.4$. We deduce that the number of modes increases with the length d_2 of the grafted resonator.

In this part, we focus on the confined modes, also known as eigenmodes, of a cell comprising a waveguide grafted by a resonator. Fig. 3(a) shows the variation of the reduced frequency as a function of the resonator length d_2. The black branches represent the transmission maxima of our system. For each value of the resonator length, one or more discrete modes corresponding to a specific frequency are obtained. These discrete modes appear as $\Omega = 0$, meaning when the resonator length is zero. As the length of the resonator increases, we observe that the discrete modes shift towards lower frequencies, and the number of discrete modes also increases. The frequencies of transmission zero, which correspond to total reflection rate of signals (Fig. 3(b)), are associated with the discrete eigenmodes of the

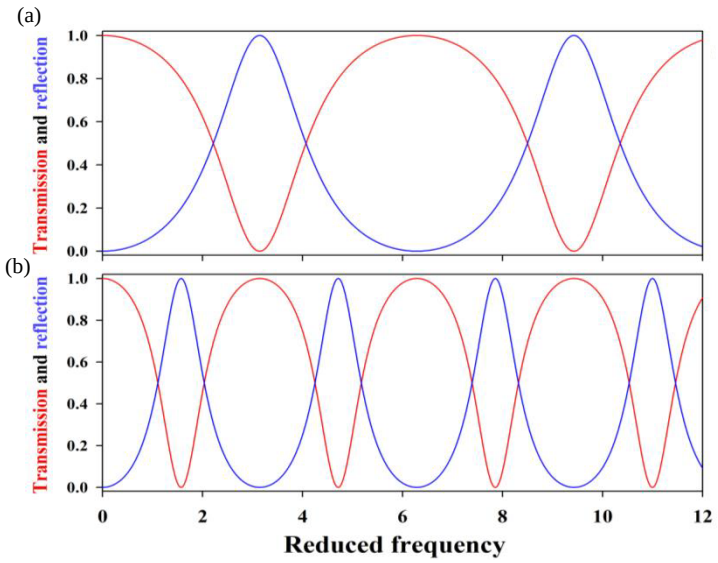

FIGURE 2. Evolution of transmission and reflection rates as a function of the reduced frequency, with (a) $d_2 = 0.5D$ and (b) $d_2 = 1D$.

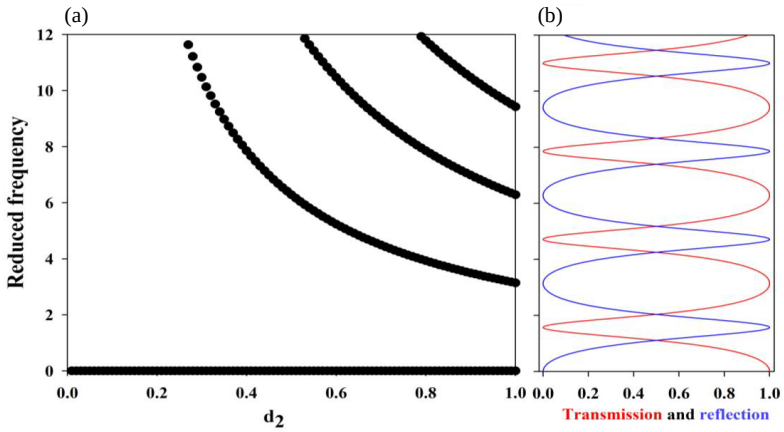

FIGURE 3. (a) Variation of the reduced frequency as a function of the resonator length d_2. (b) Variation of reduced frequency as a function of transmission and reflection rates for $d_1 = 1D$ and $d_2 = 1D$.

resonator. These eigenmodes allow selective filtering of signals. By adjusting the length of the resonator, specific transmission or reflection frequencies can be selectively filtered. Such behavior has been observed in [25].

3.2. Spectra of Transmission and Reflection in the Case of a Waveguide Grafted with Two Crossed Resonators (Cross-Shaped Structure)

In this subsection, we examine the transmission and reflection in a simple photonic device consisting of a waveguide of length d_1 and two resonators of lengths d_2 and d_3, grafted at the same site along a waveguide (Fig. 1(b)). This setup is essential for understanding the propagation of electromagnetic waves in the structure shown in the same figure, in order to obtain the Electromagnetically Induced Transparency (EIT) resonance.

Figure 4 illustrates the variation of reflection (blue line) and transmission (red line) rates as a function of the reduced frequency Ω for two resonator lengths: $d_2 = d_3 = 0.46D$ (Fig. 4(a)) and $d_2 = d_3 = 0.54D$ (Fig. 4(b)) with $d_1 = 1D$. These figures indicate the maximum and minimum values for reflection and transmission rates. Fig. 4(a) shows that transmission rate is maximum around the reduced frequencies at $\Omega = 6.29$ and falls to zero at $\Omega = 3.17$ and $\Omega = 9.4$, with the inverse occurring for reflection rate. According to Fig. 4(b), transmission rate is maximum at frequencies $\Omega = 5.84$ and $\Omega = 11.62$. We conclude that the number of modes increases with the lengths of the grafted resonators.

Figure 5 shows the variation of transmission rate (T) and reflection rate (R) as a function of the reduced frequency Ω for two different values of d_2 and d_3, while maintaining the waveguide length $d_1 = 1D$. In Fig. 5(a) ($d_2 = 0.46D$ and $d_3 = 0.51D$) and Fig. 5(b) ($d_2 = 0.46D$ and $d_3 = 0.54D$), we observe that the indicated resonances are called Electromagnetically Induced Transparency (EIT) type. EIT resonances are characterized by their symmetrical profiles, presenting line shapes that are mirror images of each other on either side of the axis to provide complete transmission at particular frequencies.

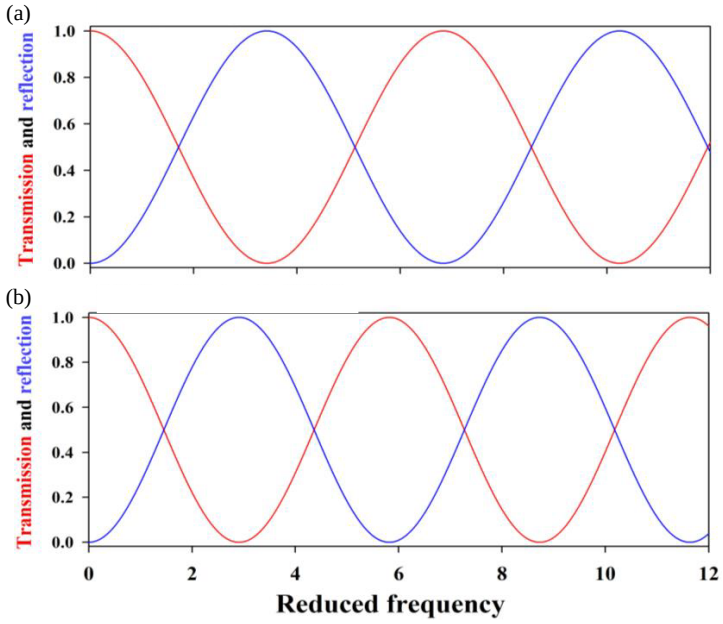

FIGURE 4. Evolution of transmission and reflection rates as a function of the reduced frequency. (a) $d_1 = 1D$, $d_2 = d_3 = 0.46D$; (b) $d_1 = 1D$, $d_2 = d_3 = 0.54D$.

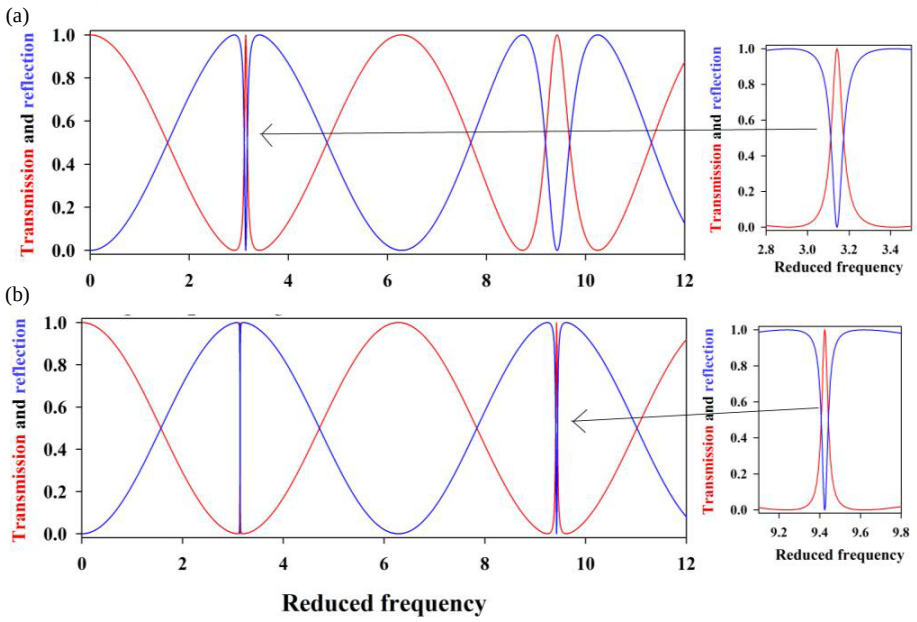

FIGURE 5. Variation of transmission and reflection rates as a function of the reduced frequency Ω, with (a) $d_2 = 0.46D$ and $d_3 = 0.51D$, $d_2 = 0.46D$ and (b) $d_3 = 0.54D$.

A particular characteristic of these resonances is the positioning of the peak, which is wedged by two transmission zeros. This specific resonance design is obtained using two different resonator lengths.

We conclude that the disappearance of the Fano mode depends on the presence of symmetrical resonators, while its emergence is associated with the presence of antisymmetrical resonators. This result has already been demonstrated by Mouadili et al. [17] when the existence of this effect is observed using the Green's function method in their study of a photonic demultiplexer.

In this part, we focus on the confined modes of a system composed of a waveguide grafted with two crossed resonators (Fig. 2(a)), with $d_1 = 1D$ and $d_3 = 0.54D$. Fig. 6(a) explores the variation of the reduced frequency as a function of the resonator length d_2, where the black branches indicate the transmission maxima. For each resonator length, one or more discrete modes corresponding to specific frequencies are identified. These branches appear as $\Omega = 0$, suggesting the presence

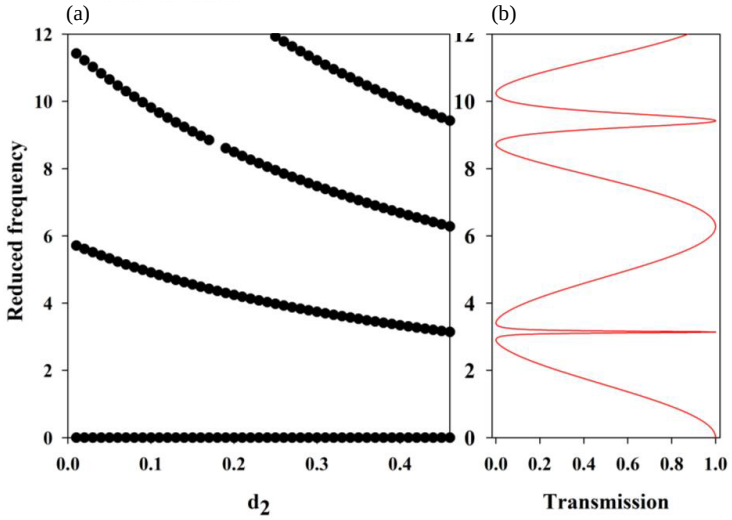

FIGURE 6. (a) Variation of the reduced frequency as a function of the resonator length d_2. (b) Variation of the reduced frequency versus the transmission rate, with $d_1 = 1D$ and $d_3 = 0.54D$.

of discrete modes even for zero resonator lengths. Increasing the resonator of length d_2 leads to a shift of discrete modes to lower frequencies, with a simultaneous increase in the number of discrete modes.

Figure 6(b) illustrates a phenomenon known as electromagnetically induced transparency resonance (EIT). This particular effect is produced when certain resonance modes of the system interact constructively, enabling high transmission at these specific frequencies. The EIT effect is characterized by its ability to create a window of transparency in a normally opaque medium, an essential aspect in photonic research and applications.

We will now explore the impact of material properties. The following spectra illustrate the transmission as a function of the reduced frequency (Fig. 7), while maintaining the lengths of the waveguide and resonators as: $d_1 = 1D$, $d_2 = 0.46D$, and $d_3 = 0.54D$. The permittivities of mediums 1 and 3 are identical, $\varepsilon_1 = \varepsilon_3 = 2.3$ (polyethylene), while we vary the value of the permittivity of medium 2 (ε_2). We clearly see that the peaks are located in the same frequency ranges, but with a slight variation in the full width at half-maximum (FWHM) of each peak.

These results demonstrate that the value of the permittivity of medium 2 has a significant influence on transmission characteristics. In particular, small changes in FWHM of each peak can be attributed to the impact of the permittivity of medium 2 on the propagation of electromagnetic waves. The variation of permittivity affects the speed of wave propagation in medium 2, leading to changes in transmission profiles. These variations are clearly reflected in the observed spectra, underlining the crucial role of permittivity in determining transmission behavior in photonic systems.

Figure 8 illustrates the coupling of the three spectra shown in Fig. 7, showing the differences between the filtered modes and their shift towards lower frequencies. This observation underlines the role of the material in filtered resonance. In this case, the optimum result is obtained when the material has a permittivity $\varepsilon_2 = 2.3$. This specific material can be used in the construction of components or coatings that require minimal interferences or attenuation of signals in these frequency ranges. The clear delimitation of modes and their frequency shifts observed in the spectra provides valuable indications for the design of photonic devices with focused frequency response characteristics.

Figure 9 shows the relation between the reduced frequency of resonant modes and permittivity ε_2, as well as the progression of transmission as a function of the reduced frequency. In Fig. 9(a), the black branches indicate the transmission maxima of the resonant modes, and we note that these transmission maxima increase as the permittivity ε_2 increases. These resonant modes represent discrete phenomena occurring at specific frequencies. The figure also shows a cutoff frequency, indicated by a particular value of the reduced frequency. Below this cutoff frequency, wave propagation is impeded, implying that resonant modes do not occur below this frequency, and signal transmission is considerably attenuated. Fig. 9(b) shows that transmission rate varies versus the reduced frequency, with $d_1 = 1D$, $d_2 = 0.46D$, and $d_3 = 0.54D$. In summary, Fig. 9 effectively shows how the reduced frequency of resonant modes varies as a function of permittivity ε_2, showing an increase in transmission maxima with higher permittivity. It also shows the progression of transmission as a function of the reduced frequency, allowing the analysis of how signal transmission varies in different frequency ranges.

3.3. Transmission Spectrum: U-Shaped Structure Based on Fano and EIT Resonances

In this subsection, we examine a system composed by two grafted resonators at two different sites and connected with waveguides (Fig. 1(c)). This system gives rise to the phenomena of Fano and Electromagnetically Induced Transparency (EIT) resonances.

Figure 10 shows two transmission spectra: one calculated using the transfer matrix method (Fig. 10(a)) and the other using

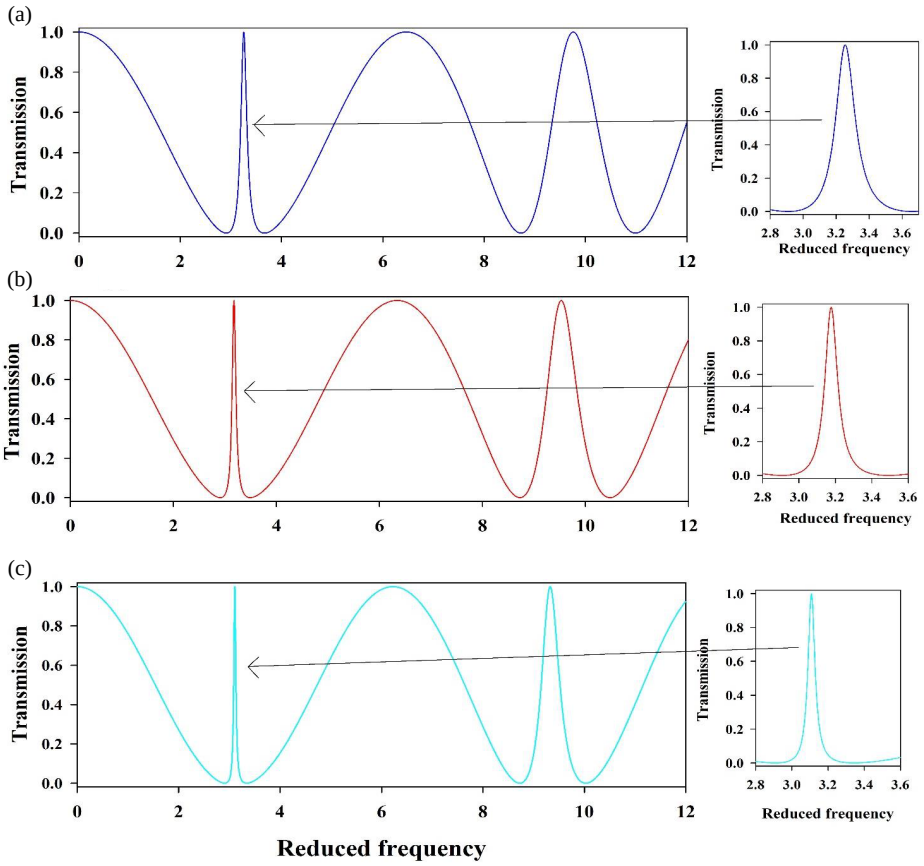

FIGURE 7. Variation the transmission rate as a function of the reduced frequency for different values of permittivity ε_2: (a) $\varepsilon_2 = 2$, (b) $\varepsilon_2 = 2.2$ and (c) $\varepsilon_2 = 2.4$.

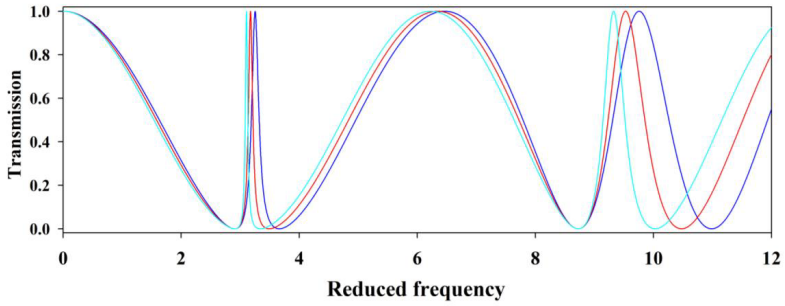

FIGURE 8. Coupling of three spectra represented Fig. 7.

Green's function method (Fig. 10(b)). Both figures show the existence of Fano resonances, which result from the constructive interferences between discrete resonances and the continuous spectrum of waveguide modes. Fig. 10(a) represents a theoretical model, and Fig. 10(b) validates the theoretical predictions by Green's function method [6], with the theoretical model being illustrated by the solid line and experimental points by the open circles. A close comparison shows small variations in peaks and resonance amplitudes between the two curves, attributable to differences in calculation approaches and experimental constraints, thus highlighting the consistency and variability of the modeled phenomena.

Figure 11 presents the variation of the transmission and reflection rates as a function of the reduced frequency Ω for various resonators of lengths d_2 and d_4. In Fig. 11(a), setting $d_1 = d_2 = d_3 = d_4 = 1D$ produces resonances characterized by high transmission rates and low quality factors. In contrast, Fig. 11(b), with $d_1 = d_3 = 1D$ and $d_2 = d_4 = 0.46D$, shows a resonance identified as Fano type due to asymmetric profile, with a maximum transmission peak near $\Omega = 3.26$ and a transmission zero at $\Omega = 3.34$. In Fig. 11(c), with $d_1 = d_3 = 1D$, $d_2 = 0.46D$, and $d_4 = 0.54D$, a resonance peak at $\Omega = 3.15$ is observed between two transmission zeros at $\Omega = 3$ and $\Omega = 3.2$. This resonance is called EIT resonance, where a transparent peak is wedged between two transmission zeros.

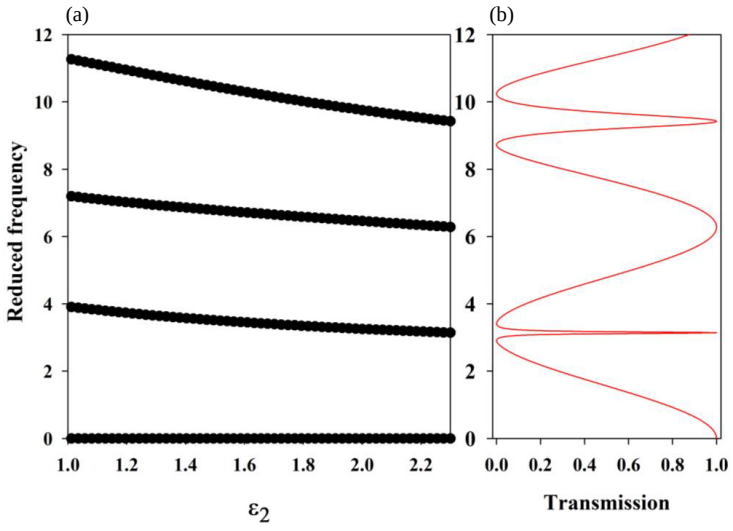

FIGURE 9. Variation of the reduced frequency of resonant modes as a function of the permittivity ε_2, with $d_1 = 1D$ and $d_3 = 0.54D$.

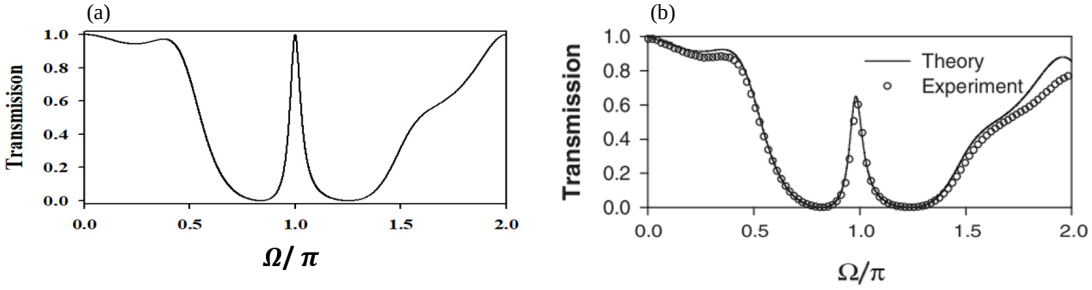

FIGURE 10. Comparative transmission spectra obtained by different methodologies: (a) Transfer Matrix Method. (b) Green's function method and experimental data [6].

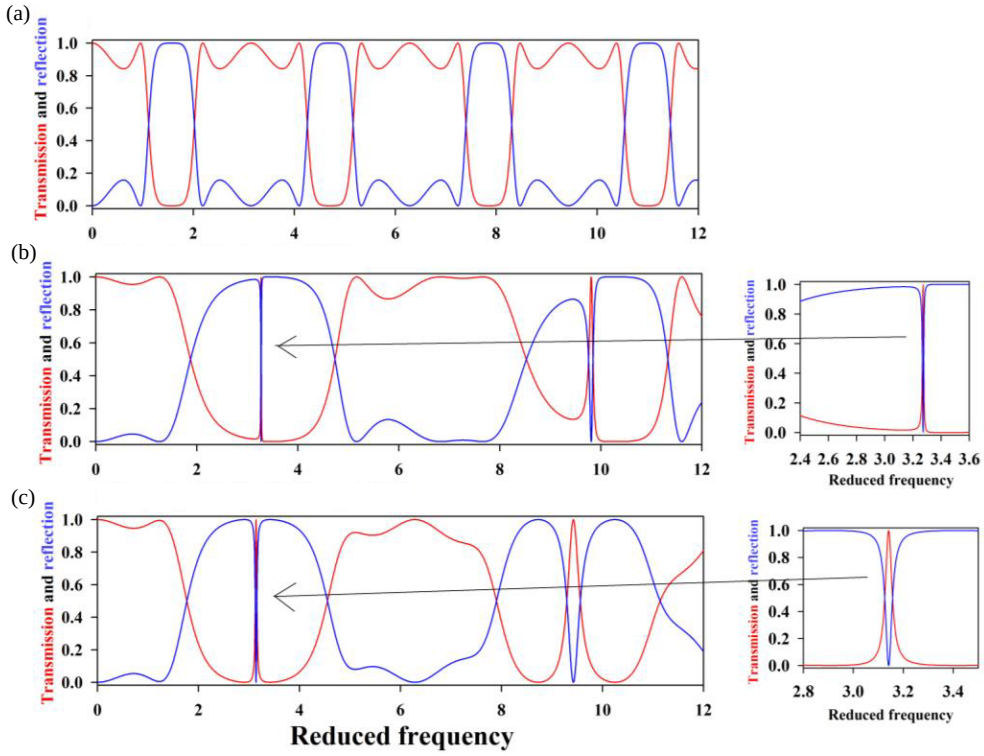

FIGURE 11. Variation of the transmission and reflection rates as a function of the reduced frequency Ω.

The principal distinction between Fano and EIT resonances in a frequency spectrum is the shape of the transmission profile: Fano resonance exhibits an asymmetrical profile, while EIT resonance displays a symmetrical bell-shaped curve. It is important to note that resonator lengths, coupling strength, and intrinsic material properties can influence the type of resonance. These results are similar to those found by Mouadili et al. using the Green's function method [6].

4. CONCLUSION

In summary, we examined the effect of resonator length for a structure composed of a guide and a resonator, finding that different resonator lengths lead to different results, giving us a better understanding of their influence on the system. Then, we studied a cross-shaped structure composed of two resonators grafted onto the same site, demonstrating that this structure produces a single type of resonance, known as the EIT resonance. Then, we turned our attention to another U-shaped structure and examined the effect of resonator lengths. Our results showed that this structure generates two types of resonance called Fano and EIT resonances. This discovery has enabled us to better understand the properties of this complex structure. This article highlights the crucial importance of the transfer matrix method in the calculation of photonic transmission using waveguides formed by coaxial cables. The transfer matrix method offers a powerful, and accurate method for analyzing and evaluating the performance of these systems in order to obtain transmission and reflection coefficients.

REFERENCES

[1] Fano, U., "Effects of configuration interaction on intensities and phase shifts," *Physical Review*, Vol. 124, No. 6, 1866–1878, 1961.

[2] Fleischhauer, M., A. Imamoglu, and J. P. Marangos, "Electromagnetically induced transparency: Optics in coherent media," *Reviews of Modern Physics*, Vol. 77, No. 2, 633–673, 2005.

[3] Harris, S. E., "Electromagnetically induced transparency," *Physics Today*, Vol. 50, No. 7, 36–42, 1997.

[4] Khattab, M. S., T. Touiss, I. E. Kadmiri, F. Z. Elamri, and D. Bria, "Multi-channel electromagnetic filters based on EIT and Fano resonances through parallel segments and asymmetric resonators," *Progress In Electromagnetics Research Letters*, Vol. 115, 105–109, 2023.

[5] El-Aouni, M., Y. Ben-Ali, I. E. Kadmiri, and D. Bria, "Electromagnetically induced transparency and Fano resonances base on coaxial photonic waveguide made up of asymmetric loop and resonators," *Key Engineering Materials*, Vol. 927, 178–188, 2022.

[6] Mouadili, A., E. H. E. Boudouti, A. Soltani, A. Talbi, A. Akjouj, and B. Djafari-Rouhani, "Theoretical and experimental evidence of Fano-like resonances in simple monomode photonic circuits," *Journal of Applied Physics*, Vol. 113, No. 16, 164 101–164 101–11, 2013.

[7] Mouadili, A., E. H. E. Boudouti, A. Soltani, A. Talbi, B. Djafari-Rouhani, A. Akjouj, and K. Haddadi, "Electromagnetically induced absorption in detuned stub waveguides: A simple analytical and experimental model," *Journal of Physics: Condensed Matter*, Vol. 26, No. 50, 505901, 2014.

[8] He, M., Q. Wang, H. Zhang, J. Xiong, X. Liu, and J. Wang, "Analog electromagnetic induced transparency of T-type Si-based metamaterial and its applications," *Physica Scripta*, Vol. 99, No. 3, 035506, 2024.

[9] Wei, B. and S. Jian, "Analogue of electromagnetically-induced-transparency based on graphene nanotube waveguide," *Journal of Physics D: Applied Physics*, Vol. 50, No. 35, 355101, 2017.

[10] Wang, B., Q. Zeng, S. Xiao, C. Xu, L. Xiong, H. Lv, J. Du, and H. Yu, "Low-power, ultrafast, and dynamic all-optical tunable plasmon induced transparency in two stub resonators side-coupled with a plasmonic waveguide system," *Journal of Physics D: Applied Physics*, Vol. 50, No. 45, 455107, 2017.

[11] Wang, Y., Z. Li, and F. Hu, "Analog of electromagnetically induced transparency at terahertz frequency based on a bilayer-double-H-metamaterial," *Journal of Physics D: Applied Physics*, Vol. 51, No. 2, 025103, 2017.

[12] Zhang, K., C. Wang, L. Qin, R.-W. Peng, D.-H. Xu, X. Xiong, and M. Wang, "Dual-mode electromagnetically induced transparency and slow light in a terahertz metamaterial," *Optics Letters*, Vol. 39, No. 12, 3539–3542, 2014.

[13] Zhu, L., X. Zhao, L. Dong, J. Guo, X. J. He, and Z. M. Yao, "Polarization-independent and angle-insensitive electromagnetically induced transparent (EIT) metamaterial based on bi-air-hole dielectric resonators," *RSC Advances*, Vol. 8, No. 48, 27 342–27 348, 2018.

[14] Chen, T., T. Xiang, J. Wang, T. Lei, and F. Lu, "Double E-shaped toroidal metasurface with high Q-factor Fano resonance and electromagnetically induced transparency," *AIP Advances*, Vol. 11, 095011, 2021.

[15] Ghaffarivardavagh, R., J. Nikolajczyk, S. Anderson, and X. Zhang, "Ultra-open acoustic metamaterial silencer based on Fano-like interference," *Physical Review B*, Vol. 99, No. 2, 024302, 2019.

[16] Miroshnichenko, A., "Fano resonances in light scattering by finite obstacles," in *Fano Resonances in Optics and Microwaves*, 473–495, Springer, 2018.

[17] Mouadili, A., E. H. E. Boudouti, A. Soltani, A. Talbi, K. Haddadi, A. Akjouj, and B. Djafari-Rouhani, "Photonic demultiplexer based on electromagnetically induced transparency resonances," *Journal of Physics D: Applied Physics*, Vol. 52, No. 7, 075101, 2018.

[18] Ben-Ali, Y., I. E. Kadmiri, Z. Tahri, and D. Bria, "High quality factor microwave multichannel filter based on multi-defectives resonators inserted in periodic star waveguides structure," *Progress In Electromagnetics Research C*, Vol. 104, 253–268, 2020.

[19] Errouas, Y., Y. Ben-Ali, I. E. kadmiri, Z. Tahri, and D. Bria, "Propagation of electromagnetic waves in one dimensional symmetric and asymmetric Comb-like photonic structure containing defects," *Materials Today: Proceedings*, Vol. 31, S16–S23, 2020.

[20] Ben-Ali, Y., Z. Tahri, F. Falyouni, and D. Bria, "Study about a filter using a resonator defect in a one-dimensional photonic comb containing a left-hand material," in *Proceedings of the 1st International Conference on Electronic Engineering and Renewable Energy*, 146–156, Springer, Singapore, 2018.

[21] Errouas, Y., Y. Ben-Ali, I. E. Kadmiri, Z. Tahri, and D. Bria, "Electromagnetic and photonic properties of materials," *J. Mater. Today Proc.*, Vol. 31, S16–S23, 2020.

[22] Ben-Ali, Y., I. E. Kadmiri, Z. Tahri, and D. Bria, "Studies in electromagnetic and photonic materials," *J. Mater. Today Proc.*, Vol. 27, 3042–3050, 2020.

[23] Touiss, T., Y. Errouas, I. E. Kadmiri, and D. Bria, "Electromagnetic filtering with high performance by one dimensional defective Comb-like waveguides structure using the transfer matrix," in *E3S Web of Conf.*, Vol. 469, 00091, 2023.

[24] Touiss, T., S. Machichi, Y. Errouas, I. E. Kadmiri, F. Falyouni, and D. Bria, "Comparative study of photonic defective Comb-like structure by the Green function and the transfer matrix method," in *E3S Web of Conf.*, Vol. 469, 00044, 2023.

[25] El Kadmiri, I., Y. Ben-Ali, A. Khaled, and D. Bria, "Y-shaped branch structure using asymmetric resonators for phononic demultiplexing," *Materials Today: Proceedings*, Vol. 27, 3033–3041, 2020.